Nuclear morphogenesis: forming a heterogeneous nucleus during embryogenesis

Albert Tsai[1,†] & Justin Crocker[1,†].
1 European Molecular Biology Laboratory, Heidelberg, Germany
† Co-corresponding authors: A.T. albert.tsai@embl.de J.C. justin.crocker@embl.de

Summary statement

We observed spatial rearrangements in the nucleus during embryo development, progressively forming a heterogeneous nuclear environment, paralleling the increasing complexity of the embryo body as morphogenesis progresses.

Abstract

An embryo experiences progressively complex spatial and temporal patterns of gene expression that guide the morphogenesis of its body plan as it matures. Using super-resolution fluorescence microscopy in *Drosophila melanogaster* embryos, we observed a similar increase in complexity in the nucleus: the spatial distributions of transcription factors became increasingly heterogeneous as the embryo matured. We also observed a similar trend in chromatin conformation with the establishment of specific histone modification patterns. However, transcription sites of specific genes had distinct local preferences for histone marks separate from the average nuclear trend, depending on the time and location of their expression. These results suggest that reconfiguring the nuclear environment is an integral part of embryogenesis and that the physical organization of the nucleus a key element in developmental gene regulation.

Introduction

During embryogenesis, transcriptional regulation controls the expression of genes that determine the fate of cells, ultimately leading to the patterning of the animal body plan (Long et al., 2016; Mallo and Alonso, 2013; Reiter et al., 2017; Spitz and Furlong, 2012). This regulatory process involves complex interactions between

transcription factors, chromatin regulators, and genome topology. Large-scale consortia have applied a variety of techniques to characterize chromatin structure and transcription factor occupancy in many cell types and tissues (Consortium, 2012; Johnson et al., 2007; Kundaje et al., 2015; Stunnenberg et al., 2016; Thurman et al., 2012). Such genome-wide assays have revealed a diversity of functional regulatory elements and the factors that bind them. Notably, as the gene expression profile of the embryo changes during cellular differentiation, genomics assays have detected wide-ranging reorginizaitons within the nucleus. Specifically, longer range interactions may bring together chromatin regions and genes into domains, as suggested by the apparance of Topologically Associated Domains (TADs) and their impact on transcriptional regulation. These observations suggest that cellular differentiation involves transforming a nucleus from a uniform compartment into a heterogeneous and partitioned space with many specialized transcriptional microenvironments.

However, these aggregate maps represent signals averaged over populations of cells and therefore mask cellular and regulatory heterogeneity. In developing embryos, this obscures the diverse cellular identities that are established and maintained. There is now recognition that cell-to-cell variation within tissues of transcription factors, chromatin modifications, and physical interactions between regulatory elements are critical for animal development (Furlong and Levine, 2018; Shema et al., 2019; Tanay and Regev, 2017). Therefore, single-cell and single-gene epigenomic analysis are required to parse the mechanisms of gene regulation across development and disease. However, a significant challenge in the field is to pair single-cell techniques with complex tissues, devolpmental systems, and regulatory models of cell-type differentiation. Methods that directly measure the natural cell-to-cell variation within tissues, non-uniform distribution of transcription factors, and chromatin states at native transcriptional elements are required.

Improvements in imaging technology—including dyes, probes, resolution, and throughput—are advancing capabilities for measuring regulatory interactions in developmental systems at the single cellular and single locus level (Chen et al., 2018; Garcia et al., 2013; Lim et al., 2018; Mir et al., 2017, 2018; Tsai et al., 2017). These imaging techniques can spatially resolve genome regulation at high resolution (Bintu et al., 2018; Mateo et al., 2019; Shema et al., 2019), opening the door to direct observations of the local transcriptional environments around individual gene loci in specific cells. We have previously found that the distributions of transcription factors are

heterogeneous in nuclei of *Drosophila* embryos in a late stage of developmentand that genes such as *shavenbaby* (*svb*) reside in regions enriched for transcription factors when they are transcriptionally active (Tsai et al., 2017). Residing in the correct local transcriptional environment is likely important for the efficient and specific expression of genes such as *svb*, whose complex regulatory regions include many enhancers utilizing low-affinity binding sites.

However, the origins and functional properties of these subnuclear transcriptional microenvironments during development remains unclear. When do transcriptional microenvironment form in the nucleus? How are these microenvironments affecting transcriptional regulation? In this survey of the transcriptional environment of the nucleus during development, we imaged the distributions of transcription factors and histone modifications in *Drosophila melanogaster* embryos at different stages of development and in different locations in the embryo. Additionally, we imaged the levels of histone modifications at *hunchback* and *rhoNEE* enhancer-driven transcription sites to follow how the regulatory preferences of a gene changes when it is expressed at different stages of embryo development and in different locations on the embryo. In sum, we found that specific nuclear environments are associated with active transcription and that the nuclear space becomes progressively more heterogeneous as development proceeds, paralleling macroscopic morphogenesis of the whole embryo. This change in nuclear organization could alter the regulatory properties of cells at different locations and times during embryogenesis, allowing dynamic and non-equilibrium processes to facilitate the increasingly complicated patterns in later stages of embryogenesis.

Results

Transcription factor distributions become more heterogeneous as development progresses

Hunchback (Hb) is a transcription factor that is active through multiple developmental stages and serve different functions. It is a gap gene in the early embryo, establishing the classical pattern (Figure 1A) immediately following cellularization (stage 5). Hb expression moved into neuroblasts (Figure 1B, stage 8) and eventually into the ventral nerve cord (Figure 1C, stage 14) as the embryo matured. The overall pattern

localized from a broad pattern spanning multiple cells in the early embryo into individual nuclei of a specific cellular lineage. To investigate if the sub-nuclear distribution of Hb also changes during development, we imaged Hb distributions in fields of nuclei showing Hb expression across three different developmental stages using high-resolution confocal microscopy with AiryScan and super-resolution STED microscopy. Figure 1D-F shows images of from the STED imaging experiments. At stage 5 (Figure 1D), the average concentration of Hb across the nucleus was generally high, but uniformly distributed across the entire nucleus. At stage 8 (Figure 1E), Hb is no longer evenly distributed, instead showing distinct nuclear regions of higher and lower Hb concentrations. At stage 14 (Figure 1F), this heterogeneity has progressed further, with regions of very high Hb concentration (similar to that of stage 5) juxtaposed next to regions with almost no Hb intensity.

As a rough quantification for the spatial distributions of Hb, we computed the autocorrelation of Hb intensity (Figure 1G). The relative levels of correlation at a given length indicates spatial structures/features at that length scale. AiryScan images were used for their wider field of view compared to STED, in order to include a larger number of nuclei. There was a monotonous increase in the level of correlation as the embryo ages, suggesting that localized Hb concentrations spanning several hundred nanometers became more prevalent as development proceeded. We also imaged Krüppel (Kr) distributions across similar developmental stages and computed their autocorrelation functions (Figure S1A). There was also a general upward trend in the level of correlation, suggesting the formation of local transcription factor environments. However, the exact functional form at each stage is different compared to Hb, suggesting that there are variations between how different transcription factors are localized in the nucleus.

Other transcription factors active within a limited time frame during development, such as Ultrabithorax (Ubx, Figure S1B) and Engrailed (En, Figure S1C) showed a jump in their autocorrelation function between when they are first expressed and when they reach maximum expression in the nuclei of cells in the ectoderm (stage 10 until stage 14, using STED imaging). Their autocorrelation functions decreased at stage 16, when the cells no longer expressed them and their distributions became very sparse. In sum, the nuclear distributions of Hb and Kr, which are active from early to late developmental stages, went from uniform to heterogeneous, whereas distributions of transcription factors (Ubx and En) that are only active later during

development only show the latter pattern. This suggests that the distributions of transcription factors become more heterogeneous as development progresses, potentially reflecting a change in the nuclear architecture.

Localized histone modifications become established during development

Because transcription factors interact with the chromatin to regulate transcription, we suspected that the state of the chromatin would influence where these factors localize within the nucleus. Several works have associated active regions of the chromatin with more open conformations, whereas repressed chromatin tend to be condensed (Boettiger et al., 2016; Szabo et al., 2018)(Figure S1D). We therefore imaged the distributions of several histone modifications associated with specific transcriptional states using high-resolution confocal microscopy to track how their spatial distributions change as embryos age. We imaged in regions showing transcription sites from a reporter construct driven by the *hunchback* (*hb*) *cis*-regulatory region on a bacterial artificial chromosome (*hbBAC*, see "Fly lines" in Materials and methods). We imaged embryos at stages 5 and 10, where nuclei transcribing from the *hbBAC* construct are within 20 µm of the surface of the embryo to preserve optimal optical resolution. We stained for H3K4me1 (Figure 2A, marking enhancers), H3K4me3 (Figure 2B, marking promoters), H3K27ac (Figure 2C, marking active promoters and enhancers), H3K36me3 (Figure 2D, marking active gene bodies) and H3K27me3 (Figure 2E, marking transcriptionally repressed regions).

In general, the trend was an increasing amount of histone modifications as the embryo ages, as seen in the increased intensities in Figure 2A-E between stages 5 and 10. The most drastic change was with the repression mark H3K27me3, which went from barely detectible to many regions of very high intensities. The autocorrelation functions of the histone modification signals in Figure 2F-J showed that histone marks also become spatially more expansive, with all marks showing increased correlation throughout all length scales. H3K27me3 (Figure 2J) showed the largest amount of change followed by H3K4me3 (Figure 2G), with the other modifications showing more moderate increases. Overall, histone modifications became established and more heterogeneous in older embryos. While there was a moderate increase in histone modifications indicating active transcription, repressive modifications showed a striking increase, forming large high-intensity regions in the nucleus.

Temporally dependent changes in the levels of histone modifications around *hunchback* transcription sites

The changing histone modification patterns during embryogenesis could alter the histone environments around genes active across multiple developmental stages, such as *hunchback* (*hb*). We therefore imaged how the levels of different histone modifications around *hb* transcription sites change in embryos of two different ages. To obtain strong fluorescence signals for histone modifications using immunofluorescence (IF) staining, we employed a staining method that do not require a denaturing step common in many RNA fluorescence *in situ* hybridization (RNA FISH) (Figure 3A, see "Immunofluorescence staining" in Materials and methods). In brief, we crossed a *Drosophila melanogaster* line expressing a reporter mRNA containing MS2 stem loops driven by a BAC containing the *cis*-regulatory region of *hb* to another line that contains MCP-GFP to label the mRNA with GFP. The mRNA transcription signal was then amplified using IF staining, in conjunction with staining for histone modifications. With this method, we obtained strong signals for both the transcription sites and for histone modifications (for example Figure 3B-E for H3K4me1 and H3K27me3). The *hb* transcription sites appeared in a radial band toward the anterior of stage 5 embryos and in neuroblasts along cells that would become the ventral nerve cord in stage 10 embryos.

To quantify the spatial distribution of histone marks around transcription sites, we computed the average radial intensity distribution function centered on the intensity maximum of the transcription site (Figure 3F-J), using the method described in (Tsai et al., 2017), and described in "Image processing" in Materials and methods. The histone environment around active *hb* transcription sites showed specific patterns of change that deviated from the global trend of histone distributions presented in Figure 2. Specifically, we observed a clear increase in H3K4me1 signal around *hb* transcription sites going from stage 5 to stage 10 embryos (Figure 3F), while H3K4me3 (Figure 3G) only showed a small increase. This is the opposite for the global distributions of these marks (Figure 2F & G), where the increase in H3K4me3 correlation was higher. H3K27ac (Figure 3H) did not change between stage 5 and 10, but H3K36me3 (Figure 3I) intensity showed a moderate increase. Interestingly, many of the active histone modifications showed an initial dip in intensity at the transcription sites, but quickly increased to their maximum values within 200 to 300 nm. The repressive

mark H3K27me3 (Figure 3J) showed a different functional form from active marks, with no initial dip and a gentle downward slope. There were no changes between stages 5 and 10, despite the general strong increase in repressive histone modifications throughout the nucleus going from stage 5 to 10 (Figure 2J). The specific increase in H3K4me1 around *hb* transcription sites could indicate the inclusion of more distal regulatory elements in older embryos. The relatively unchanged H3K4me3 intensity profile would suggest that proximal regulatory elements, including the promoter, are in use in both the early and late stages of development.

Spatially dependent changes in the local histone environment at *rho* transcription sites

As we observed changes in the local histone environment as a function of time, we investigated if the local histone modification levels could also have spatial dependence on the location of the cell. The *rho* enhancer drives expression in an anterior to posterior band along the side of stage 5 embryos (Figure 4A). The sharp ventral edge of the *rho* pattern results from Snail repression and the pattern trails off gradually in the dorsal direction due to a decreasing gradient of the activator Dorsal (Figure 4B). While most transcriptionally active cells are in the active region (Figure 4C, Active), some nuclei expressing from the *rho* enhancer could still be observed in the repressed region (Figure 4C, Rep.) using a similar method for tracking *hb* (see “Fly lines” in Materials and methods).

We quantified the level of H3K4me1 marking enhancers and H3K4me3 marking promoters at the transcription site (Figure 4D), sorting cells based on their location in the *rho* expression pattern (e.g. Figure 4E & F). We observed that transcription sites in the active region had a higher level of H3K4me1 compared to sites in the repressed region (Figure 4G, $p < 0.05$, two-tailed Student’s t-test). In contrast, there was no difference for H3K4me3 (Figure 4H), with transcription sites in both regions having similar levels. While the difference in H3K4me1 could be due to regulatory actions from the *rho* enhancer due to the levels of the Snail repressor, H3K4me3 levels could be explained by the reporter construct containing a poised promoter. Thus, our results show that local levels of histone modifications could report on the state of regulatory elements, which may differ depending on the time and place of expression, even for the same gene.

Discussion: Increasing heterogeneity in the nucleus could be an integral part of embryogenesis

During development, the embryo undergoes changes in its transcriptional profiles, adapting to the different regulatory needs for each step of embryogenesis (Figure 4I & J). In early embryos, cell division occur quickly and transcription factors form concentration gradients spanning the embryo with relatively uniform intra-nuclear distributions (Figure 4I). This early stage lasts approximately 6 hours in *D. melanogaster* embryos. Subsequently, the division rate slows down and the detailed segmentation of the body plan takes place. This phase lasts several times longer, requiring approximately 18 hours. During this phase, many regulatory and signaling pathways controlling the development of different cell types and organs become active, leading to a complicated regulatory environment in the nucleus (Figure 4J). We observed that the expression patterns of transcription factors became cell-specific and their distributions within the nucleus, heterogeneous. Especially for transcription factors that regulate different genes during later stages of development, physical separation from early genes in the nucleus can prevent their inadvertent activation.

As transcription factor binding depends interacting with DNA, this partitioning of their nuclear distribution could reflect a change in the chromatin environment. In eukaryotes, DNA is wrapped around histones, whose amino acid residues on their CTD tails can be modified with a variety of marks. These modifications are linked to different states of transcriptional regulation and chromatin accessibility. Starting from the end of the early stages of embryo development in *Drosophila*, when zygotic gene expression turns on, the levels of several histone modifications rapidly increase in specific places on the genome. This occurs concurrent to the establishment of higher order structures, such as topologically associating domains (TADs) and to the chromatin organizing into distinct transcriptionally active or repressed regions. We observed such increases in active and repressive histone modifications in post zygotic transition embryos, forming local sub-nuclear compartments enriched for these marks. These regions are large compared to individual gene loci, spanning approximately several hundreds of nanometers, sufficient to encompass multiple genes. The increase in the repressive mark H3K27me3, closely associated with the polycomb group proteins (Denholtz et al., 2013), was the most drastic, which could be differentiating cells shutting down genomic regions. This change in chromatin organization could create distinct

accessibility patterns on the chromatin, guiding transcription factors into heterogeneous distributions in older embryos.

These changes in the distributions of transcription factors and chromatin states could alter the regulation of specific genes depending on their position in the nucleus. For example, we observed an increase in a histone modification associated with active enhancers (H3K4me1) near active *hb* transcription sites between stage 5 and 10 embryos. In contrast, the levels of H3K4me3 associated with active promoters were high in both younger and older embryo. The rapid division cycle and relative lack of structure in the nucleus in the early embryo might mean that genes in the early embryo preferentially utilize proximal regulatory elements due to kinetic constraints. As the nuclear environment becomes more stable and heterogeneous in older embryos, long-distance interactions could form and introduce distal regulatory elements. For genes active during multiple developmental stages, this physical separation permits them to respond to different regulatory inputs and serve multiple roles using the same *cis*-regulator region. Moreover, we observed a similar trend in space for the transcription sties from the *rho* enhancer, where changing H3K4me1 but constant H3K4me3 suggest an active promoter but differential engagement from the enhancer element. Together, these results imply that the histone environments around genes could be different depending on the states and contributions of different *cis*-regulatory elements. These differences could provide the basis for refining the expression pattern over time, as is the case for many developmental genes (Briscoe and Small, 2015), where local differences in epigenetic marking around the gene could guide incorrectly expressing or silent cells into their proper state.

This survey of the distributions of transcription factors and histone modifications across several developmental stages of *Drosophila* embryos has provided a preliminary view into the emergence of a heterogeneous nucleus during development. In a way, this nuclear process mirrors the increasingly complex patterns that control morphogenesis across the entire embryo. This shift in the nuclear environment highlights the importance of directly observing gene regulation in older embryos (i.e. beyond the switchover to zygotic expression and even gastrulation). Lineage-, location-, and time-specific observation of the environments around individual genes in embryos could yield insights into how kinetics of gene regulation differ between older and younger embryo. It would also be important to expand to other developmental systems across the

evolutionary tree to confirm the generality and to discover the evolutionary origins of using sub-nuclear compartmentalization as a strategy for transcriptional regulation. It could be that increasing heterogeneity across different length scales, from the nucleus to the embryo body plan, is a hallmark of embryo development and other complex processes in eukaryotes.

Materials and methods

Fly lines

All *Drosophila melanogaster* strains were maintained under standard laboratory conditions at 23 °C. *D. melanogaster* containing the *cis*-regulatory region of *hunchback* (*hb*) on a bacterial artificial chromosome (BAC) driving a *yellow* reporter mRNAs containing 24 MS2 stem loops generated in (Bothma et al., 2015) was used as a readout for the expression of *hb*. The reporter construct for *rho* is derived from the plasmid pIB-hbP2-P2P-lacZ-αTub3 UTR (Chen et al., 2012) with the hbP2 region between the restriction sites HindIII and AscI replaced with the *rhoNEE* sequence. The plasmid was synthesized by Genscript (Piscataway, New Jersey, USA). The construct was injected into Bloomington Drosophila Stock Center line 27388 and integrated using RMCE by GenetiVision (Houston, Texas, USA). Virgin flies from a transgenic *D. melanogaster* line containing MS2 coat protein (MCP) fused with eGFP driven by the *nanos* promoter from (Garcia et al., 2013) was crossed with the *hbBAC* or the *rho* reporter line to label the transcriptions sites for further amplification using immunofluorescence (IF) staining. The MCP-GFP line does not contain a nuclear localization signal (NLS) to minimize MCP-GFP forming aggregates in the nucleus in the absence of MS2 mRNAs.

Enhancer sequence for *rhoNEE*

CTTGGGCAGGATGGAAAAATGGGAAAACATGCGGTGGGAAAAACACACATCGCGAAACATTTGGCGCAACTTGCGGAAGAC
AAGTGCGGCTGCAACAAAAAGTCGCGAAACGAAACTCTGGGAAGCGGAAAAAGGACACCTTGCTGTGCGGCGGGAAGCGCA
AGTGGCGGGCGGAATTTCCTGATTCGCGATGCCATGAGGCACTCGCATATGTTGAGCACATGTTTTGGGGGAAATTCCCGGGC
GACGGGCCAGGAATCAACGTCCTGTCCTGCGTGGGAAAAGCCCACGTCCTACCCACGCCCACTCGGTTACCTGAATTCGAGCT

Immunofluorescence staining

Embryos from w^{1118} flies (for imaging transcription factors) and from crosses of the *hbBAC* or *rho* reporter line with the MCP-GFP line (for imaging transcription sites and histone modifications) were collected, fixed and stained

using the protocols in (Crocker et al., 2015; Tsai et al., 2017). Primary antibodies were detected using secondary antibodies labeled with Alexa Fluor dyes (at a dilution ratio of 1:500, Invitrogen) for confocal and Airyscan imaging. Transcription sites, Hb and Kr were imaged using Alexa488 and the rest with Alexa555. For STED microscopy, secondary antibodies with Alexa594 (1:500, Invitrogen) or STAR RED (1:250, Abberior) were used. Ubx was imaged using Alexa594 and the rest using STAR RED.

The primary antibodies and their dilution ratios were:

Hb: Generated for the Berkeley Drosophila Transcription Network Project (Li et al., 2008), (1:100)

Kr: Generated for the Berkeley Drosophila Transcription Network Project (Li et al., 2008), (1:100)

Ubx: Developmental Studies Hybridoma Bank, FP3.38-C, (1:20)

En: Santa Cruz Biotechnology, (d-300), sc-28640, (1:50)

GFP: ThermoFisher, GFP Monoclonal Antibody (3E6), A-11120, (1:500)

H3K4me1: Merck, Anti-monomethyl-Histone H3 (Lys4) Antibody, 07-436, (1:250)

H3K4me3: Cell-Signaling Technology, Tri-Methyl-Histone H3 (Lys4) (C42D8) Rabbit mAb, 9751, (1:250)

H3K27ac: Active Motif, Histone H3K27ac antibody (pAb), 39133, (1:250)

H3K27me3: Active Motif, Histone H3K27me3 antibody (pAb), 39157, (1:250)

H3K36me3: abcam, Anti-Histone H3 (tri methyl K36) antibody, ab194677, (1:250)

Confocal and Airyscan microscopy

Confocal and Airyscan imaging follow the protocols in (Tsai et al., 2017). Specifically, mounting of fixed Drosophila embryos was done in ProLong Gold + DAPI (Molecular Probes, Eugene, OR). Fixed embryos at the appropriate stage and orientation were imaged on a Zeiss LSM 880 confocal microscope with FastAiryscan (Carl Zeiss Microscopy, Jena, Germany). Excitation lasers with wavelengths of 405, 488 and 561 nm were used as appropriate for the specific fluorescent dyes. Whole-embryo overviews were imaged using a Zeiss LD LCI Plan-Apochromat 25x/0.8 Imm Korr DIC M27 objective. High resolution confocal and Airyscan stacks were imaged using a Zeiss Plan-Apochromat 63x/1.4 Oil DIC M27 objective. The optimal resolution as recommended by the Zen software from Zeiss was used for the x-y (70.6 nm for confocal and 42.5 nm for Airyscan) and z direction (320 nm for confocal and 190 nm for Airyscan) of stacks used for quantification. The laser power and gain were adjusted to maximize the signal to noise ratio within the dynamic range of the PMT or Airyscan detector. The acquired Airyscan stacks were processed with Zen 2.3 SP1 (Carl Zeiss Microscopy, Jena, Germany) in 3D mode to obtain super-resolved images.

STED microscopy

Mounting of fixed Drosophila embryos was done in ProLong Diamond without DAPI (Molecular Probes, Eugene, Oregon, USA). Fixed embryos at the appropriate stage and orientation were imaged on a STEDYCON (Abberior Instruments, Göttingen, Germany) in 2D STED mode on an Olympus BX53 microscope (Olympus, Tokyo, Japan). Excitation lasers with wavelengths of 594 and 640 nm were used as appropriate for the specific fluorescent dyes. The wavelength of the STED laser was 775 nm. All samples were imaged using an Olympus UPlanSApo 100X Oil/1.4 objective. The resolutions used for the x-y and z direction were 25 nm and 250 nm, respectively. The laser power and gain were adjusted to maximize the signal to noise ratio within the dynamic range of the APD detector on the STEDYCON.

Image processing

Image processing was done using Fiji (Schindelin et al., 2012) with the 3D ImageJ Suite plugin (Schmid et al., 2010). Image processing to obtain radially averaged intensity distributions around transcription sites was done according to (Tsai et al., 2017), with the following modification to signal normalization: for each transcription site, the

maximum intensity measured in the entire radial distribution is normalized to 1, instead of normalizing to the intensity value at $r = 0$. Radially averaged autocerrelation functions were computed using an ImageJ macro (imagejdocu.tudor.lu/macro/radially_averaged_autocorrelation). Intensity distributions and autocorrelation fuctions were plotted using Matlab (MathWorks, Natick, MA).

Acknowledgements

The *hunchback* BAC line was a generous gift from Michael Levine. The MCP-eGFP line and the plasmid pIB-hbP2-P2P-lacZ-αTub3 UTR were generous gifts from Hernan Garcia. The Hunchback and Krüppel primary antibody were generous gifts from Mark Biggin. We would like to thank Marko Lampe at the EMBL Advanced Light Microscopy Facility for his expert advice and training to conduct STED imaging. We would also like to thank members of the Crocker Group for valuable discussions and suggestions to improve the manuscript.

Funding

Albert Tsai is supported by the German Research Foundation (Deutsche Forschungsgemeinschaft, TS 428/1-1).

Albert Tsai and Justin Crocker are supported by the European Molecular Biology Laboratory (EMBL).

Data and Material Availability

The original images (AiryScan, confocal, and STED) will be available for download and are indexed at: https://www.embl.de/download/crocker/XXXXX. All fly lines and plasmid sequences will be available upon reasonable request.

References

Bintu, B., Mateo, L.J., Su, J.H., Sinnott-Armstrong, N.A., Parker, M., Kinrot, S., Yamaya, K., Boettiger, A.N., and Zhuang, X. (2018). Super-resolution chromatin tracing reveals domains and cooperative interactions in single cells. Science (80-.). *362*.

Boettiger, A.N., Bintu, B., Moffitt, J.R., Wang, S., Beliveau, B.J., Fudenberg, G., Imakaev, M., Mirny, L.A., Wu, C., and Zhuang, X. (2016). Super-resolution imaging reveals distinct chromatin folding for different epigenetic states. Nature *529*, 418–422.

Bothma, J.P., Garcia, H.G., Ng, S., Perry, M.W., Gregor, T., and Levine, M. (2015). Enhancer additivity and non-additivity are determined by enhancer strength in the Drosophila embryo. Elife *4*.

Briscoe, J., and Small, S. (2015). Morphogen rules: design principles of gradient-mediated embryo patterning. Development *142*, 3996–4009.

Chen, H., Xu, Z., Mei, C., Yu, D., and Small, S. (2012). A System of Repressor Gradients Spatially Organizes the Boundaries of Bicoid-Dependent Target Genes. Cell *149*, 618–629.

Chen, H., Levo, M., Barinov, L., Fujioka, M., Jaynes, J.B., and Gregor, T. (2018). Dynamic interplay between enhancer–promoter topology and gene activity. Nat. Genet. *50*, 1296–1303.

Consortium, T.E.P. (2012). An integrated encyclopedia of DNA elements in the human genome. Nature *489*, 57–74.

Crocker, J., Abe, N., Rinaldi, L., McGregor, A.P.P., Frankel, N., Wang, S., Alsawadi, A., Valenti, P., Plaza, S., Payre, F., et al. (2015). Low affinity binding site clusters confer hox specificity and regulatory robustness. Cell *160*, 191–203.

Denholtz, M., Bonora, G., Chronis, C., Splinter, E., de Laat, W., Ernst, J., Pellegrini, M., and Plath, K. (2013). Long-range chromatin contacts in embryonic stem cells reveal a role for pluripotency factors and polycomb proteins in genome organization. Cell Stem Cell *13*, 602–616.

Furlong, E.E.M., and Levine, M. (2018). Developmental enhancers and chromosome topology. Science (80-.). *361*, 1341–1345.

Garcia, H.G., Tikhonov, M., Lin, A., and Gregor, T. (2013). Quantitative Imaging of Transcription in Living Drosophila Embryos Links Polymerase Activity to Patterning. Curr. Biol. *23*, 2140–2145.

Johnson, D.S., Mortazavi, A., Myers, R.M., and Wold, B. (2007). Genome-Wide Mapping of in Vivo Protein-DNA Interactions. Science (80-.). *316*, 1497–1502.

Kundaje, A., Meuleman, W., Ernst, J., Bilenky, M., Yen, A., Heravi-Moussavi, A., Kheradpour, P., Zhang, Z., Wang, J., Ziller, M.J., et al. (2015). Integrative analysis of 111 reference human epigenomes. Nature *518*, 317–330.

Li, X., MacArthur, S., Bourgon, R., Nix, D., Pollard, D.A., Iyer, V.N., Hechmer, A., Simirenko, L., Stapleton, M., Hendriks, C.L.L., et al. (2008). Transcription Factors Bind Thousands of Active and Inactive Regions in the Drosophila Blastoderm. PLoS Biol. *6*, e27.

Lim, B., Heist, T., Levine, M., and Fukaya, T. (2018). Visualization of Transvection in Living Drosophila Embryos. Mol. Cell *70*, 287-296.e6.

Long, H.K., Prescott, S.L., and Wysocka, J. (2016). Ever-Changing Landscapes: Transcriptional Enhancers in Development and Evolution. Cell *167*, 1170–1187.

Mallo, M., and Alonso, C.R. (2013). The regulation of Hox gene expression during animal development. Development *140*, 3951–3963.

Mateo, L.J., Murphy, S.E., Hafner, A., Cinquini, I.S., Walker, C.A., and Boettiger, A.N. (2019). Visualizing DNA folding and RNA in embryos at single-cell resolution. Nature *568*, 49–54.

Mir, M., Reimer, A., Haines, J.E., Li, X.-Y., Stadler, M., Garcia, H., Eisen, M.B., and Darzacq, X. (2017). Dense Bicoid hubs accentuate binding along the morphogen gradient. Genes Dev. *31*, 1784–1794.

Mir, M., Stadler, M.R., Ortiz, S.A., Hannon, C.E., Harrison, M.M., Darzacq, X., and Eisen, M.B. (2018). Dynamic multifactor hubs interact transiently with sites of active transcription in Drosophila embryos. Elife *7*.

Reiter, F., Wienerroither, S., and Stark, A. (2017). Combinatorial function of transcription factors and cofactors. Curr. Opin. Genet. Dev. *43*, 73–81.

Schindelin, J., Arganda-Carreras, I., Frise, E., Kaynig, V., Longair, M., Pietzsch, T., Preibisch, S., Rueden, C., Saalfeld, S., Schmid, B., et al. (2012). Fiji: an open-source platform for biological-image analysis. Nat Methods *9*, 676–682.

Schmid, B., Schindelin, J., Cardona, A., Longair, M., and Heisenberg, M. (2010). A high-level 3D visualization API for Java and ImageJ. BMC Bioinformatics *11*, 274.

Shema, E., Bernstein, B.E., and Buenrostro, J.D. (2019). Single-cell and single-molecule epigenomics to uncover genome regulation at unprecedented resolution (Nature Publishing Group).

Spitz, F., and Furlong, E.E.M. (2012). Transcription factors: from enhancer binding to developmental control. Nat. Rev. Genet. *13*, 613–626.

Stunnenberg, H.G., International Human Epigenome Consortium, S., Hirst, M., Almeida, M. de, Altucci, L., Amin, V., Amit, I., Antonarakis, S.E., Aparicio, S., Arima, T., et al. (2016). The International Human Epigenome Consortium: A Blueprint for Scientific Collaboration and Discovery. Cell *167*, 1145–1149.

Szabo, Q., Jost, D., Chang, J.M., Cattoni, D.I., Papadopoulos, G.L., Bonev, B., Sexton, T., Gurgo, J., Jacquier, C., Nollmann, M., et al. (2018). TADs are 3D structural units of higher-order chromosome organization in Drosophila. Sci. Adv. *4*, eaar8082.

Tanay, A., and Regev, A. (2017). Scaling single-cell genomics from phenomenology to mechanism. Nature *541*, 331–338.

Thurman, R.E., Rynes, E., Humbert, R., Vierstra, J., Maurano, M.T., Haugen, E., Sheffield, N.C., Stergachis, A.B., Wang, H., Vernot, B., et al. (2012). The accessible chromatin landscape of the human genome. Nature *489*, 75–82.

Tsai, A., Muthusamy, A.K.A.K., Alves, M.R.P.M.R., Lavis, L.D.L.D., Singer, R.H.R.H., Stern, D.L.D.L., and Crocker, J. (2017). Nuclear microenvironments modulate transcription from low-affinity enhancers. Elife *6*.

Figures

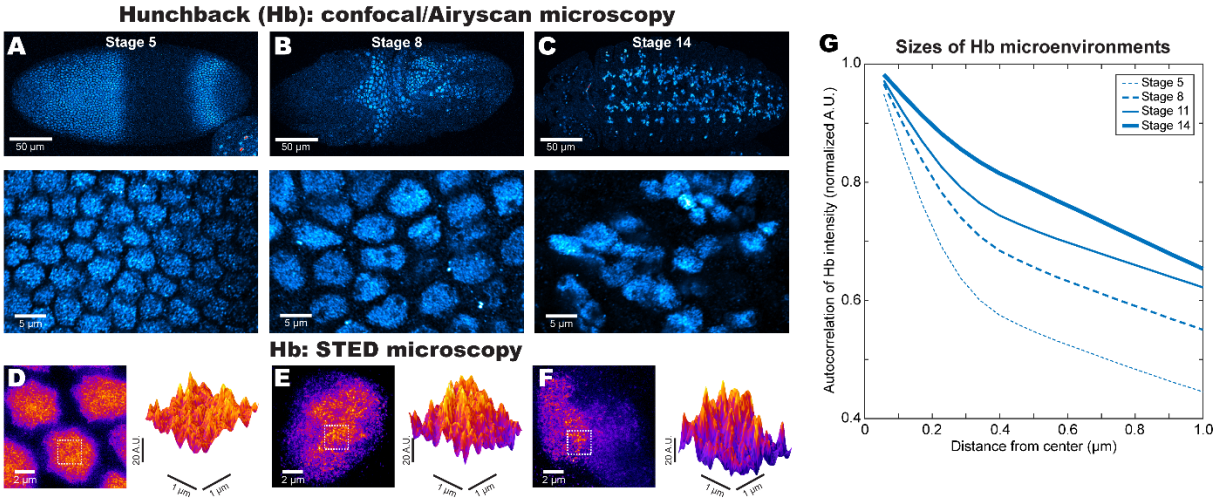

Figure 1: Increasing heterogeneity in Hb distribution as embryo development progresses

The distribution of Hb in *Drosophila* embryos goes from the classical gradient pattern in stage 5 (A, top panel), into the more specific cell lineages in stage 8 (B, top panel) and finally into cells in the nerve cord in stage 14 (C, top panel). The bottom panels in A-C show a zoomed-in view of the nuclear distribution of Hb in those stages. The top panels are confocal images and the bottom panels are Airyscan images. Superresolution imaging using STED microscopy (D-F) shows that the levels of Hb are high and uniform across the nucleus in stage 5 (D), but becomes increasingly heterogeneous as the embryo proceeds through stage 8 (E) and stage 14 (F). (G) The radially averaged autocorrelation function of Hb (using Airyscan images) quantifies the overall prevalence of spatial structures at different length scales. There is an increase in the autocorrelation function across all length scales in the various stages of embryos imaged.

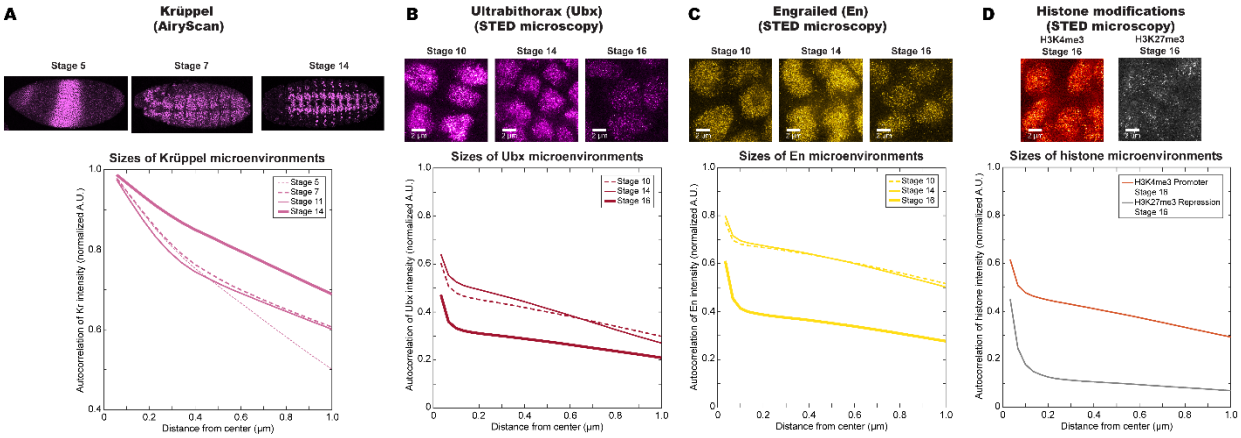

Figure S1: The spatial scales of transcription factors and histone marks as a function of embryo age and regulatory function

(A) A similar increase in the autocorrelation function compared to Hb (Figure 1G) is also observed for Krüppel across developmental stages. Transcription factors that are only expressed during later stages of embryo development, such as (B) Ubx and (C) En, do not show a uniform nuclear distribution. During stages 10 and 14, when both factors are expressed, their distributions are heterogeneous and show significant levels of autocorrelation. Their expression decreases significantly by stage 16. The physical sizes of the chromatin can vary according to their transcriptional state and accessibility, as seen in (D).

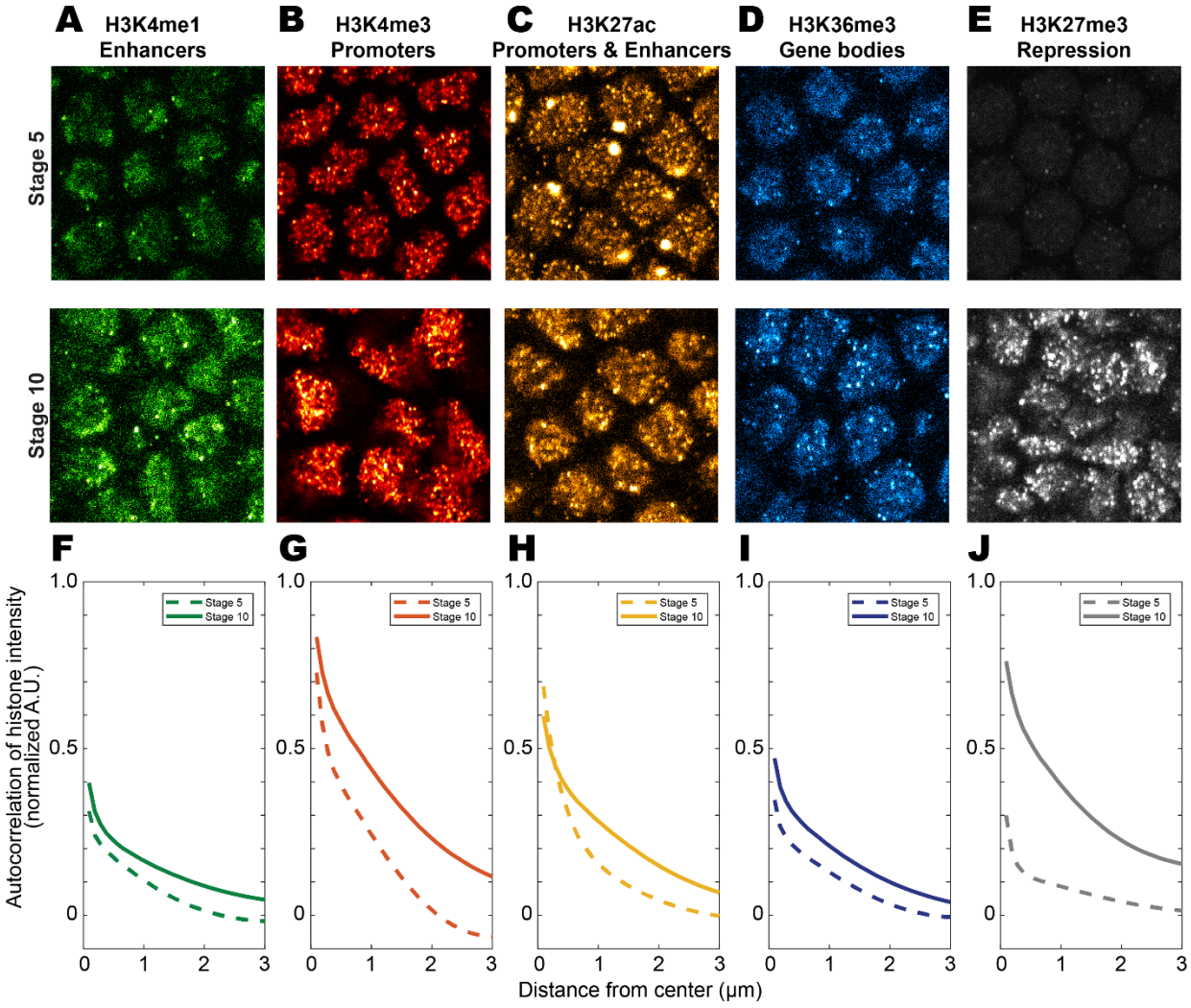

403 ## Figure 2: Increasing histone modifications as a function of embryo age

404 The chromatin shows increased levels of histone modifications as shown in (A-E) when comparing embryos at
405 stages 5 and 10: (A) H3K4me1 marking enhancers, (B) H3K4me3 marking promoters, (C) H3K27ac marking active
406 enhancers and promoters, (D) H3K36me3 marking active gene bodies, and (E) H3K27me3 marking repressed
407 regions. While the levels of many marks increased between stages 5 and 10, H3K27me3 goes from barely
408 detectable in stage 5 to having regions of very high intensities in stage 10. The autocorrelation functions (F-J) of
409 the histone modifications shows this general trend, with an increase in association across all length scales.

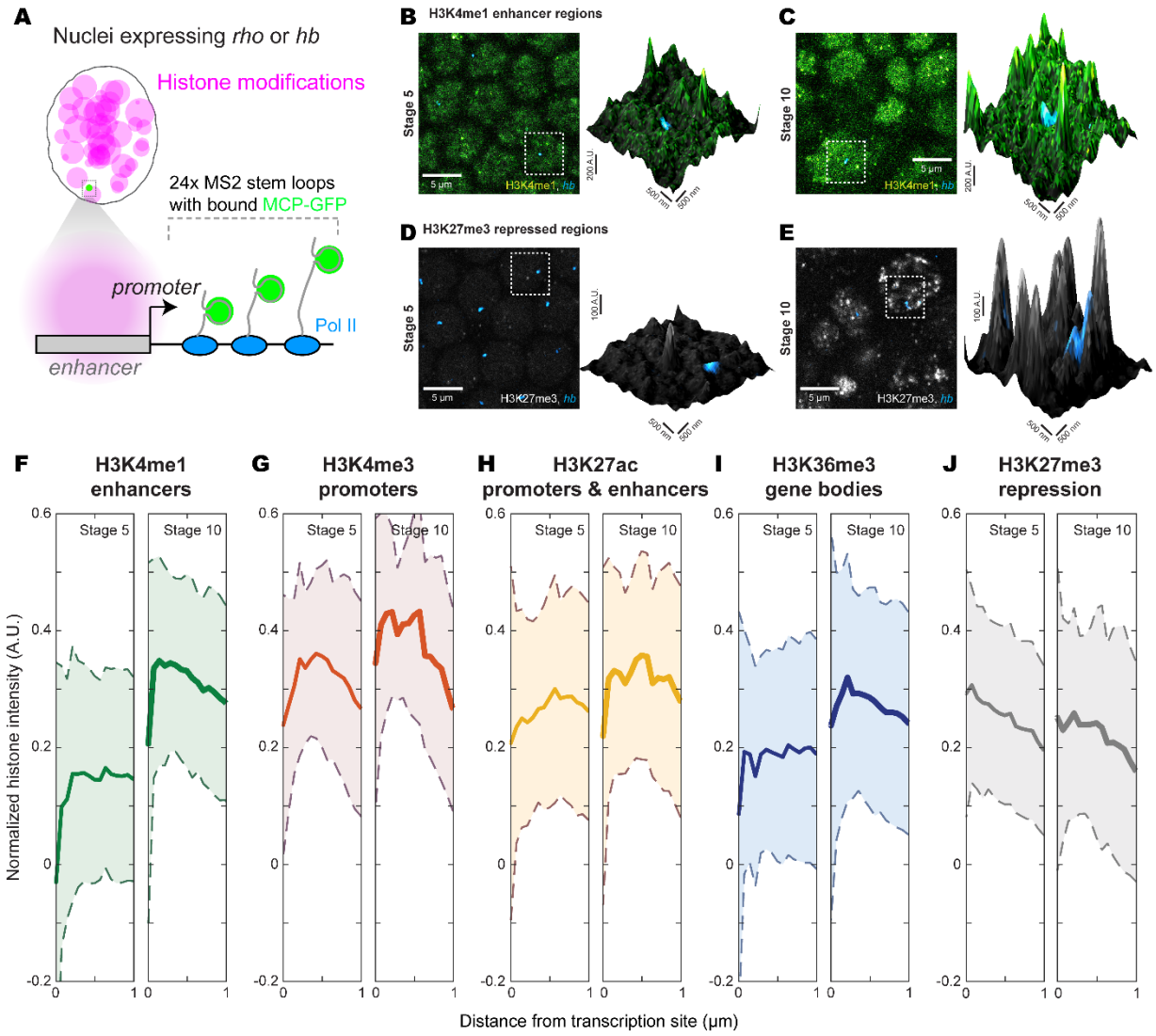

411 Figure 3: The histone environment at *hb* transcription sites depends on the timing of

412 their expression

413 (A) Marking transcription sites of a MS2 reporter gene driven by the *cis*-regulatory region of *hb* or *rho* using MCP-

414 GFP and IF amplification preserves the signal of histone modifications stained using IF. This allows the

415 simultaneous imaging of transcription sites and histone modifications with good signal-to-noise ratio (e.g. B & C for

416 H3K4me1 and D & E for H3K27me3, at stage 5 and 10 respectively). (F-J) The radially averaged distributions of

417 several histone modifications around *hb* transcription sites show changes between stages 5 and 10 that are specific

418 to these transcription sites. H3K4me1 (F) showed the strongest increase although its general increase across the

419 nucleus (Figure 2A & F) was the smallest. H3K27me3 (J) showed the opposite pattern where there is no change

420 around hb transcription sites even though it strongly increased across the nucleus (Figure 2E & J). H3K4me1: stage

421 5 n = 51 transcription sites, stage 10 n = 111. H3K4me3: stage 5 n = 69, stage 10 n = 52. H3K27ac: stage 5 n = 178,

422 stage 10 n = 63. H3K36me3: stage 5 n = 54, stage 10 n = 88. H3K27me3: stage 5 n = 235, stage 10 n = 66.

423

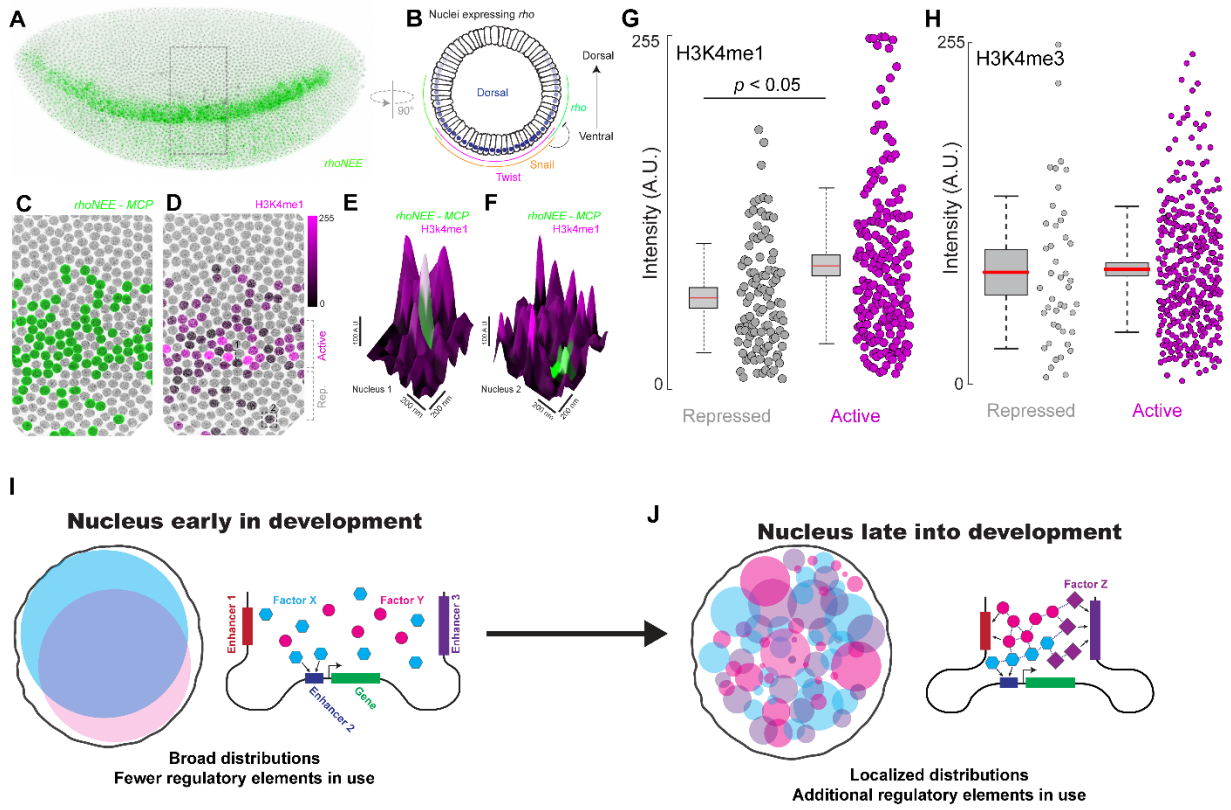

Figure 4: The histone environment at *rho* transcription sites depends on their location in the embryo

(A) The expression pattern of the *rhoNEE* enhancer on a side view of a stage 5 embryo. (B) The regulatory inputs of *rho* along the dorsal-ventral axis. (C) Zoomed panel from the box in (A) with nuclei with *rho* transcription site in green. (D) Same view as (C) with the shade of magenta depicting the intensity of H3K4me1 at the transcription site. (E & F) Zoomed in view around a transcription of a nucleus from the (E) active and (F) repressed zone of *rho* expression, with the z-axis showing H3K4me1 intensity. (G & H) Quantification of (G) H3K4me1 and (H) H3K4me3 levels at *rho* transcription sites. H3K4me1 repressed: n = 94 transcription sites, active: n = 535. H3K4me3 repressed: n = 44, active n = 354.